Materials Advances

PAPER

Check for updates

Efficient dual-phase visual detection of pesticides in real samples with electron-rich emitters carrying multiple twists†

Shivani Tripathi [ID] and Manab Chakravarty [ID] *

Precise monitoring of pesticides in daily consumable items and the environment is crucial to save society. By considering numerous challenges, such as the cost, operational difficulties, and portability of existing pesticide detection strategies, we herein introduce simple, low-cost triphenylamine (TPA)-enriched structurally diverse π-conjugates as potential dual-state emitters for rapid and visual detection of pesticides, mainly trifluralin (TN; highly toxic to aquatic animals and affects fertile soil) and fenitrothion (FN; an organophosphorus insecticide, lethal to humans on high exposure). Other pesticides, i.e., glyphosate (GP) and imidacloprid (IM), also poorly responded. The newly designed small molecules displayed intense, visually detectable emission in both solution and solid states due to the extensive π-conjugations and multiple twisted sites in the molecular structures. An increment of the TPA units increases the energy of the LUMO of the probes, and thus, the emission profiles alter in solution and solid states. However, these probes are capable of detecting TN and FN selectively through photo-induced electron transfer (PET) and inner-filter effect (IFE) mechanisms, and can be recognised through the naked eye. Among the three probes, AIEEgen **TT1** showed the maximum efficiency with a detection limit up to 180 nM due to favorable PET/IFE and its crystalline nature that would facilitate capturing the analytes in the void space. All the findings are well elucidated with experimental and theoretical support. Thus, a handy paper-based platform is presented to visually recognize TN and FN pesticide residues present in soil, fruits, and vegetables. Such an inexpensive protocol would help common people to test household items before handling them.

Introduction

The unique propeller-shaped molecular structure and opto-electronic properties of electron-rich triphenylamine (TPA) have become vital in central optical sciences.[1–7] Myriad TPA-based molecules are recognized with efficient fluorescence properties and possess very high thermal stabilities.[8–11] Many aggregation-induced emission (AIE)-active molecules are generated using such propeller-shaped TPA units that introduce multiple twisted sites within the molecules.[12–14] Thus, many solid-state emissive TPA-conjugated building blocks with excellent hole transport properties are well recognized for offering devices related to OLED or photovoltaic applications. Molecular

Department of Chemistry, Birla Institute of Technology and Sciences-Pilani, Hyderabad Campus, Jawaharnagar, Medak, Shamirpet, Hyderabad-500078, India. E-mail: manab@hyderabad.bits-pilani.ac.in

† Electronic supplementary information (ESI) available: The following files are available free of charge. Synthesis, additional characterization details, thermal analysis, powder X-ray diffraction patterns, optical properties, Thermal stability experiments, pesticide detection supportive data, NMR, and IR; all the data are included herein. See DOI: https://doi.org/10.1039/d5ma00630a

engineering with the TPA unit was very feasible due to its synthetic and conformational flexibility. Varying non-planar TPA units were well-documented for developing stimuli-responsive emitters.[15–18] Enriching TPA units in organic molecules can monitor the emission changes in the solid state by avoiding the strong π–π stacking and facilitate exhibiting AIE and solid-state emissions. TPA units can also increase the conjugation effect and create a bridge between different units to control the emission features. In this report, we have designed TPA-centered anthracenyl-linked π-conjugates (**TT1**, **TT2**, and **TT3**) holding multiple twisted sites, where the TPA units were incrementally added to the main framework, producing a 'V' shaped **TT2** and C_3-symmetric **TT3** systems with different emission profiles in the solution/solid state.

Although TPA-based emitters are widely investigated for developing various devices for real-world applications, they are hardly used to detect pesticides. The indiscriminate use of a wide range of toxic pesticides above the restricted limit is an urgent need to fulfill the global food demand. The toxicity of pesticides is a concern for the flora and fauna;[19–21] therefore, developing suitable and economic strategies to detect

pesticides becomes crucial.[22–24] Expensive chromatographic techniques linked to mass spectrometry are mainly used as analytical tools to detect pesticides,[25,26] and they require a well-equipped laboratory with expert hands. The same issues arise with sensitive electrochemical and photoelectrochemical detection of pesticides.[27–29] Therefore, highly sensitive and economical fluorescence-based detection techniques are highly praiseworthy. Many fluorescence-based techniques have been established to detect pesticides with high selectivity and sensitivity.[30–34] However, most fluorescent materials are polymeric or organic molecule-based nanocomposites, requiring multi-step, expensive, and harsh-conditioned synthetic protocols to access them.[35–40] Furthermore, multiple expensive techniques and critical analysis/speculation are needed to describe them. Despite displaying excellent sensitivity, such ill-defined molecules suffer from not offering a practical solution for pesticide detection. In this context, well-defined small molecules would be an alternative route to offer the potential for pesticide detection. Hence, we report an easy metal-free highly emissive nature of TPA-based **TT1**, **TT2**, and **TT3** molecules in the dual state (solution/solid state), which are employed to detect pesticides in a handy and visually detectable method (Fig. 1).

Notably, TPA-linked nanocomposites, meso/microporous polymeric molecules, are utilized to detect pesticides.[41–43] Reports on TPA-based small molecules are not yet recognized. Out of these three molecules, only **TT1** displayed AIEE-features; however, all these compounds **TT1**, **TT2**, and **TT3** are strongly emissive (green/yellow) in the solid state and exhibit quick visually detectable responses against trifluralin (TN, a widely used efficient herbicide) and fenitrothion (FN) (an organophosphate pesticide to kill a broad-spectrum of pests) in excellent sensitivity (10–100 nM). Furthermore, weak responses against glyphosate (GP) and imidacloprid (IM) were noticed. The solution state emission showed limited responses with only

TN and FN. However, the **TT1** among all three fluorophores showed maximum potential in both solution and solid states. The photoinduced electron transfer (PET) and inner-filter effect (IFE) possibly play a crucial role in quenching the emission. Such a solid-state emitter is successfully utilized to detect the presence of pesticides on soil, and various fresh vegetables and fruits with the help of a 365 nm lamp. In fact, these probes can detect the pesticides present on various surfaces, such as smooth leaves and rough fruit skin.

Results and discussion

Our recent development on organophosphonate chemistry to install electron-rich units *via* metal-free Friedel–Crafts (FC)-type arylation reactions motivated us to install a TPA unit to an anthracenyl core in a simple and convenient strategy.[44] Typically, the TPA unit is linked to the functionalized cores *via* expensive metal-catalyzed cross-coupling reactions under harsh conditions.[45] Notably, this is a unique approach to introduce a TPA unit using $MeSO_3H$ at 25 °C in dichloromethane (DCM) solvent, leading to the production of TPA-linked anthracenyl phosphonate (TPAP) in 84% yield. Such a phosphonate is an excellent precursor to undergo Horner–Wadsworth–Emmons (HWE) reactions with TPA-aldehyde, affording TPA-linked anthracenyl π-conjugates such as **TT1** (Scheme 1), carrying TPA units.

Furthermore, in a manner like **TT1**, TPA-units are gradually increased by reacting **TPAP** with TPA–$(CHO)_2$ and TPA–$(CHO)_3$ individually to access **TT2** (56%) and **TT3** (64%), respectively (Scheme 1). All the compounds are soluble in various organic solvents and well characterized by multinuclear NMR and mass spectrometric studies.[46] The thermal stabilities of these probes were promising (Fig. S1, ESI†) and were stable until >300 °C for **TT1**, **TT2** and **TT3**. Suitable single crystals for X-ray diffraction could not be generated for these π-conjugates, but the
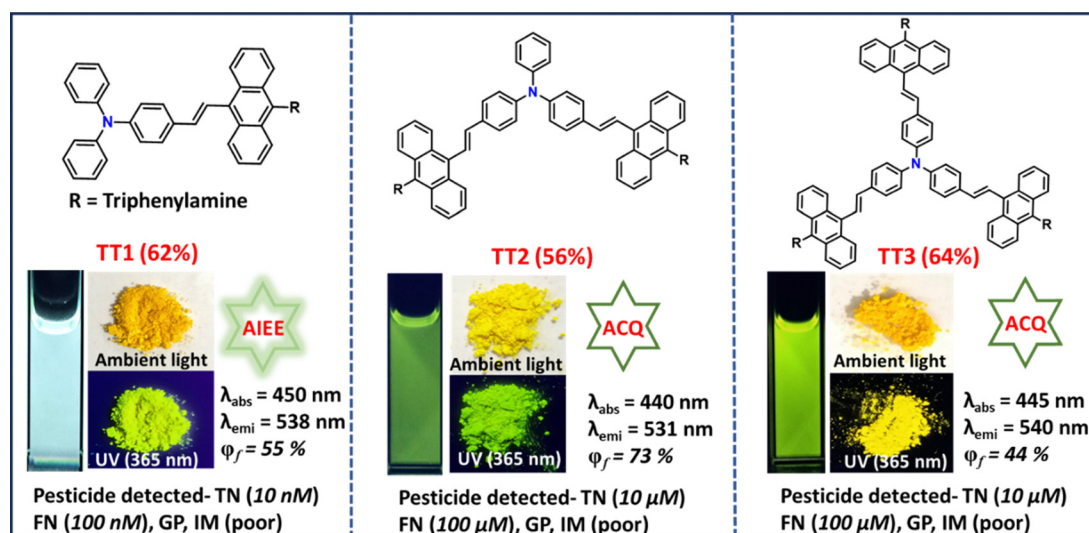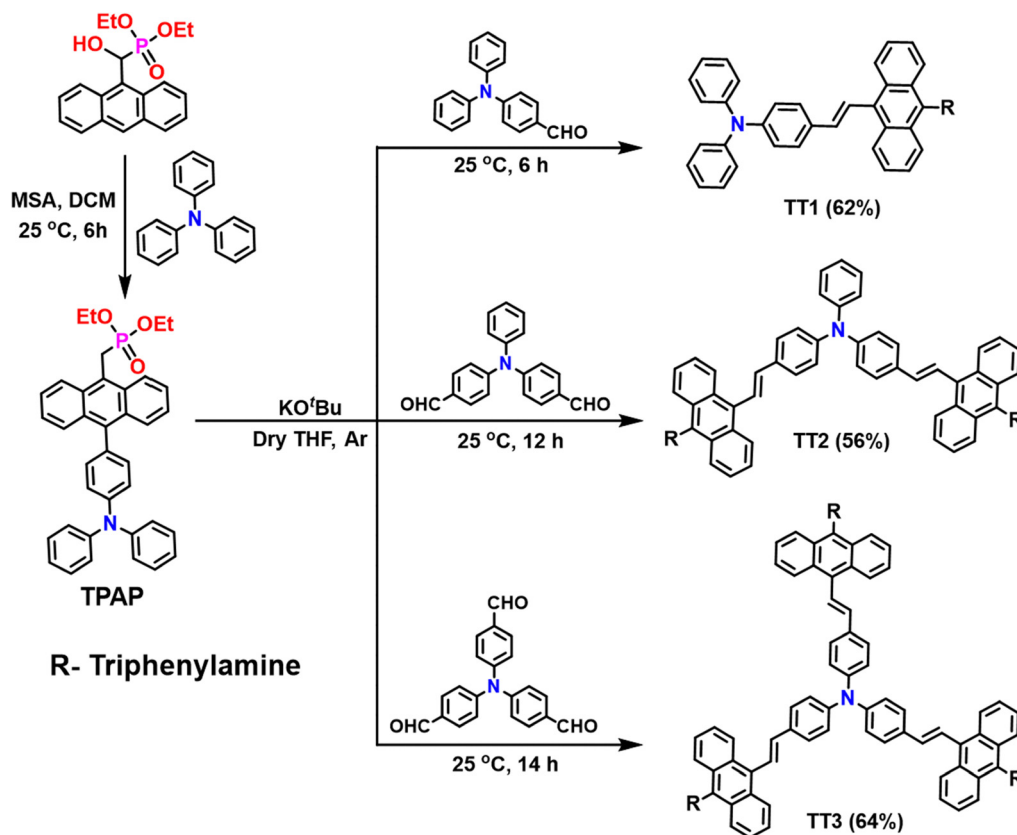

Fig. 1 The dual-state emitters and their differences in emission profiles and pesticide detections. R: triphenylamine; TN: trifluralin, FN: fenitrothion, GP: glyphosate; IM: imidacloprid.

Scheme 1 Synthesis protocol for the fluorophores **TT1**, **TT2**, and **TT3**.

powder X-ray diffraction studies indicated the crystallinity only in **TT1**; both **TT2** and **TT3** are amorphous in nature (Fig. S2, ESI†) and showcased broad peaks denoting less ordered orientation of molecules.

Photophysical properties and detection of pesticides in the solution state

The UV/vis absorption spectroscopy of **TT1** showed a strong absorption at λ_{max} 330 nm along with a small hump at 410 nm, possibly due to π–π^* transitions. The other two compounds,

TT2 and **TT3**, mainly displayed the absorption at λ_{max} = 430 nm (Fig. S3a–c, ESI†). The solvatofluorochromic studies of **TT1** revealed mostly blue emission ($\sim$410–460 nm) up to 60% quantum yield (Φ_f) in most of the solvents and were almost non-emissive in MeOH and water (Table S1, ESI†). On the other hand, both **TT2** and **TT3** exhibited emission at longer wavelengths (greenish yellow $\lambda_{max} \sim$ 530–560 nm) with decent emission (Φ_f = 20–30%) (Fig. 2i–iii and Fig. S4a–c, ESI†). These preliminary studies imply a lower conjugation in **TT1** compared to **TT2** and **TT3**, yet all the emissions were visually identified.
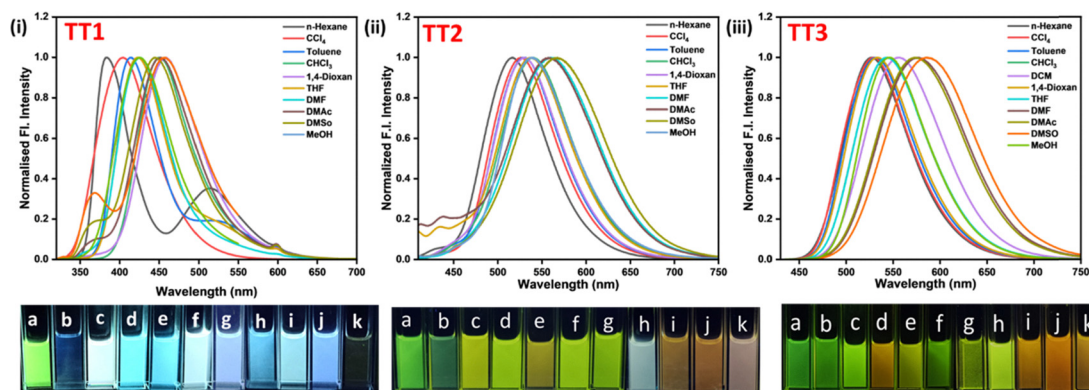

Fig. 2 The solvatochromic features of the compounds (i) **TT1**, (ii) **TT2** and (iii) **TT3**; the solvents (a) hexane, (b) carbon tetrachloride (CCl₄), (c) toluene, (d) dichloromethane (DCM), (e) chloroform (CHCl₃), (f) 1,4-dioxane, (g) tetrahydrofuran (THF), (h) N,N-dimethylformamide (DMF), (i) dimethylsulphoxide (DMSO), (j) dimethylacetamide (DMAc), and (k) MeOH.
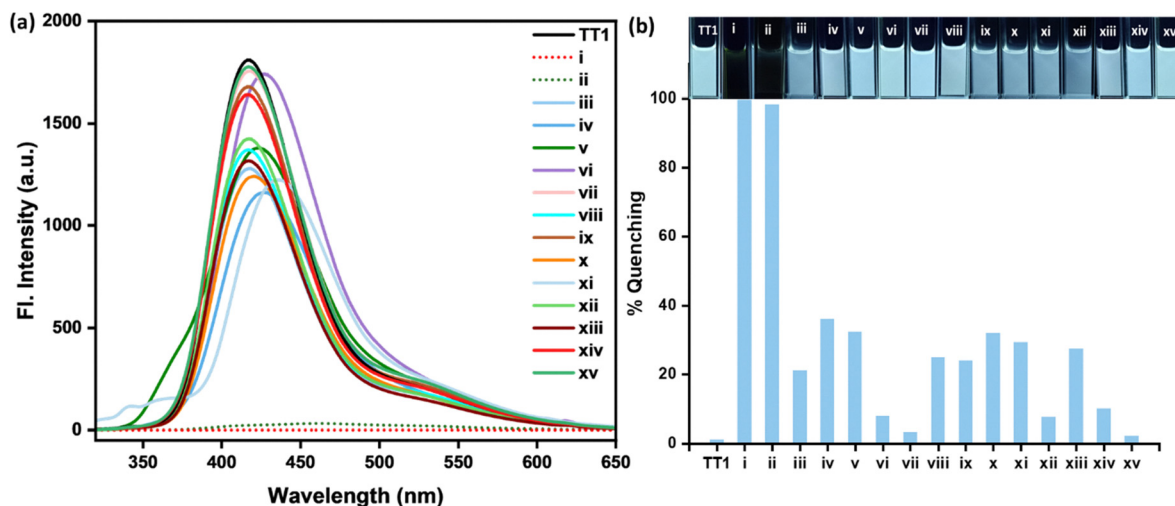
Fig. 3 (a) Emission spectra of **TT1** after adding all the analytes. (b) Bar diagram representing the % quenching of **TT1** (inset is a photograph of **TT1** (10 μM in 1,4-dioxane) after treatment with various analytes): (i) TN, (ii) FN, (iii) IM, (iv) CF, (v) CP, (vi) GP, (vii) PN, (viii) DP, (ix) sodium pyrophosphate tetrabasic, (x) dipotassium hydrogen phosphate, (xi) tricalcium phosphate, (xii) 4-nitrotoluene, (xiii) 1,2-chloro dinitrobenzene, (xiv) 2-chloro-4-nitroaniline, and (xv) diethyl benzyl phosphonate.

All these emissive solutions (10 μM in 1,4-dioxane) were separately treated with various important analytes (10 μM in 1,4-dioxane), related to agricultural usages. The analytes include crucial pesticides: trifluralin (TN), fenitrothion (FN),

imidacloprid (IM), β-cyfluthrin (CF), chlorpyrifos (CP), glyphosate (GP), permethrin (PN), and diphenylamine (DP); and vital chemicals used in certain pesticide formulations, fertilisers and building blocks for the pesticides: 1,2-chloro
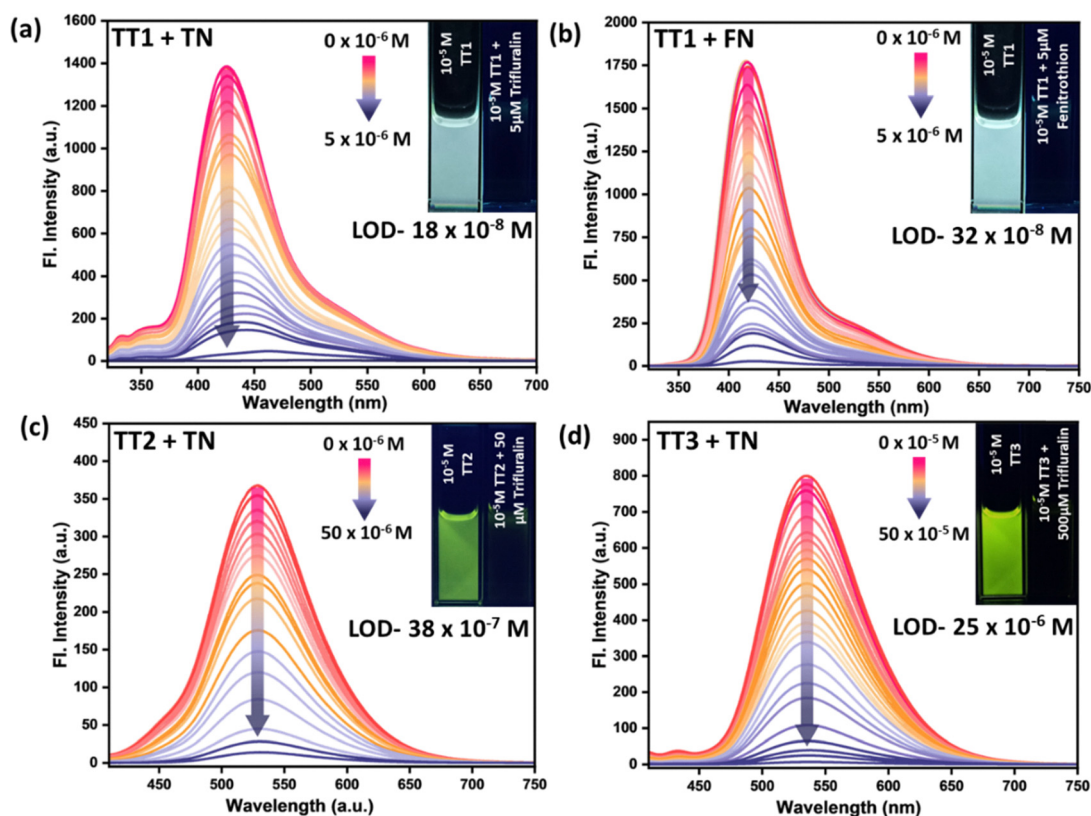

Fig. 4 Change in emission spectra (10 μM in 1,4-dioxane) by gradual addition of TN and FN: (a) **TT1** + TN (λ_{ex} = 310 nm), (b) **TT1** + FN (λ_{ex} = 310 nm), (c) **TT2** + TN (λ_{ex} = 430 nm), and (d) **TT3** + TN (λ_{ex} = 430 nm), respectively; inset pictures correspond to the emission before and after pesticide addition under 365 nm UV light.

dinitrobenzene, sodium pyrophosphate tetrabasic, dipotassium hydrogen phosphate, tricalcium phosphate, 4-nitrotoluene and 2-chloro-4-nitroaniline, and diethyl benzyl phosphonate. The blue-emissive **TT1** solution responded rapidly with emission quenching against nitro-group containing TN and FN, selectively (Fig. 3a and b). The green-emissive solution of **TT2** and **TT3** exhibited selective and efficient responses by emission disappearance against only TN (Fig. S5a–d, ESI†), and no other analytes.

Such a response with the selective pesticides motivated us to treat the pesticides TN and FN separately with these emissive solutions (Fig. 4a–d). The gradual addition of TN into 10 μM solutions of **TT1**, **TT2**, and **TT3** resulted in an enhancement in the absorption (hyperchromic); (Fig. S6a–d, ESI†) without any spectral shift, indicating the higher absorption possibly due to improved alignment between donor–acceptor molecules or changes in the molecular environment, which can perhaps enhance the transition probability. Furthermore, the absorption spectra of TN partly overlap with our probe (*vide infra*; Fig. S18, ESI†), and thus, the increased concentration of TN can also contribute to the overall absorbance enhancement. The FN pesticide was only treated with the **TT1** solution as it was selective to only **TT1**. However, a notable color change was not observed under ambient light, but the emission change was quite favorable due to emission quenching.

To find the mechanistic route, the ^{1}H-NMR spectra of **TT1** (Fig. S7, ESI†) were recorded before and after the addition of TN. The unchanged NMR spectra specify no chemical reactions/interactions between the probes and analytes, verifying that the interaction between the probes and analytes does not alter any electronic arrangement. Furthermore, the fluorometric titration was conducted to determine the Stern–Volmer constant ($K_{S–V}$). The S–V plot showed a linear relationship at lower concentrations of quencher and found an upward curvature (non-linear) upon higher quencher concentration, indicating the contribution from both static and dynamic (collision) quenching (Fig. S8a–d, ESI†). The $K_{S–V}$ (M^{-1}) was determined as 2.5×10^9 with TN, 3×10^9 with FN for **TT1**, and 2.4×10^8 with TN for **TT2**, and 2×10^7 with TN for **TT3**, respectively, considering the slope at lower concentrations (Fig. S9a–d, ESI†). It was further confirmed by excited-state lifetime measurement studies. The lifetime decay was fitted biexponentially for **TT1**, **TT2**, and **TT3** (Fig. S10, ESI†), and displayed longer excited state lifetime for **TT1** (4.52 ns) than **TT2** (1.88 ns) and **TT3** (1.78 ns). The calculated radiative rate constant ($k_r \times 10^6$ s^{-1}): 134.9 was much higher than the nonradiative rate constant ($k_{nr} \times 10^6$ s^{-1}): 86.2 only for **TT1**. For **TT2** and **TT3**, the k_{nr} was largely dominating over k_r (Table S2, ESI†), specifying the reason for the much weaker emission Φ_f. The significant reduction in the excited state lifetime upon addition of TN and FN [**TT1** + TN: 4.23 ns; **TT1** + FN: 4.43 ns; **TT2** + TN: 1.71 ns; **TT3** + TN: 1.73 ns] designates the dynamic quenching as the main cause (Fig. S11 and Table S3, ESI†). Furthermore, the lessening in lifetime after gradual addition of TN confirms the dynamic quenching (Fig. S12 and Table S4, ESI†). Thus, the emission disappearance originates from a complex quenching

mechanism. The limit of detection (LOD) was determined by the $3.3\sigma/k$ method [σ = standard error of the linear fitting and k = slope]; (Fig. S13a–d, ESI†), revealing the quenching ability of TN and FN at the level of 10^{-8} M with **TT1** emitter, while **TT2** and **TT3** could detect only TN as low as 10^{-6} and 10 μM, respectively. Thus, **TT1** is relatively more sensitive against TN pesticide compared to other TPA-enriched molecules **TT2** and **TT3**. More importantly **TT1** solution also offered the ability to recognize another broad-spectrum organophosphate pesticide, FN. The Job's plot analyses revealed a 1:1 stoichiometry between the emitters and pesticide, which causes quenching in all these cases (Fig. S14a–d, ESI†).

Dynamic quenching is ensured *via* transient interactions between fluorophores and analytes, typically mediated by photo-induced electron transfer (PET). The electron will be transferred from a photoexcited electron-rich probe to the pesticide (acceptor). Thus, the photoexcited electrons will be transferred to the lowest unoccupied molecular orbitals (LUMOs) of the analytes. All these molecules were structurally optimized using density functional theory (DFT) performed using B3LYP-D3(BJ)/6-31G** (with dispersion corrections). For **TT1**, the highest occupied molecular orbital (HOMO) was lying on the electron-rich anthracene–π–TPA part and the LUMO was built by the anthracene unit. However, the energy of E_{LUMO} (eV) for **TT1**, **TT2**, and **TT3** was determined theoretically to be −1.98, −1.80, and −1.83 eV, respectively (Fig. S15, ESI†). The rise in the number of electron-rich TPA-units enhances the E_{LUMO} energy level, as expected.

The selectivity of TN and FN can be easily elucidated by their LUMO energy (eV), located at only a lower energy than all other pesticides (Fig. S16, ESI†) used herein and facilitating an easy electron transfer from all these emitters (Fig. S15, ESI†). The LUMO energy difference between **TT1** and these two pesticides, TN and FN, is smaller than that of other probes, enabling a suitable PET, and thus is responsible for selective and sensitive detection. Based on these energy levels, **TT2** and **TT3** were also expected to exhibit responses against FN (Fig. 5 and Fig. S17, ESI†). Of note, the response was not satisfactory in the solution state. Such discrepancies are not completely understood yet but can be addressed from the difference of emission wavelength $\lambda_{em} \sim 423$ nm of **TT1** than **TT2** and **TT3**, displaying emission at $\lambda_{em} \sim 530$ nm, where the emission band of **TT1** showed an overlap with the absorption band of TN and FN, whereas the **TT2** and **TT3** emission bands showed only a trivial overlap with the TN absorption band, but the absorption band of FN had no overlap (Fig. S18a, ESI†). Additionally, no overlap was observed in the case of IM, CF, CP, GP, PN, and DP. To enhance the clarity regarding the overlapping regions contributing to the IFE, the absorbance spectra of TN and FN were simplified and presented alongside the normalised emission spectrum of **TT1**. This visualisation effectively highlights the spectral overlap responsible for the IFE phenomenon (Fig. S18b, ESI†). Thus, the IFE was present for **TT1** with TN and FN, and the combined effect of PET and IFE was responsible for such efficient quenching. However, the quenching effect was observed for both TN and FN using all these emitters in the solid state (*vide infra*).
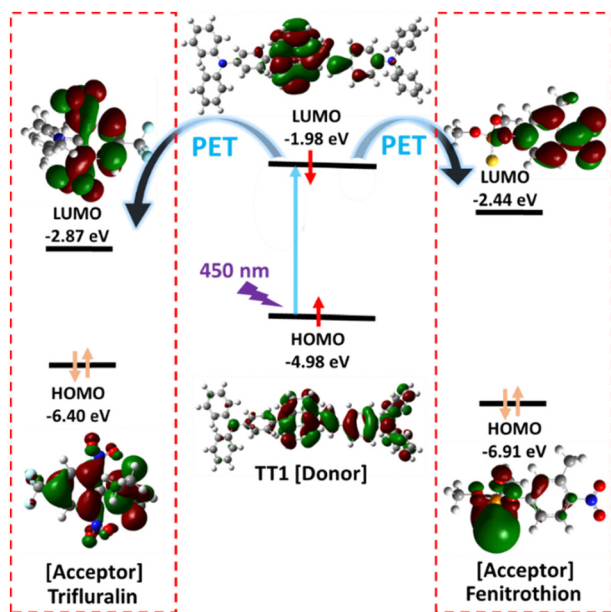
Fig. 5 Schematic diagram representing the HOMO–LUMO energy level of **TT1** with trifluralin and fenitrothion demonstrating a PET mechanism. All these energy levels are theoretically determined [B3LYP-D3(BJ)/6-31G** (with dispersion corrections)].

Solid-state emission and pesticide detection

The molecular geometry with multiple twists was expected to exhibit enhanced emission in the aggregated state.[47] Hence, the AIE-feature was tested for these molecules varying gradual water fraction (f_w) in 10 μM MeCN solution of the emitters (Fig. S19, ESI†). The emission enhancement was noticed from 40% f_w, which reached the maximum at 50% f_w. The emission intensity was diminished upon further increment of f_w. Nevertheless, **TT2** and **TT3** showed aggregation-caused quenching (ACQ) behavior upon performing similar experiments. Such an ACQ behavior for **TT2**–**TT3** can be attributed to the presence of multiple aryl/anthryl units that typically incline to form multiple supramolecular contacts, including π–π interactions in the aggregated state, which enable the emission quenching.[48–50] Furthermore, the **TT1** nanoaggregate formation at f_w = 50% was confirmed through the SEM (scanning electron microscope) and DLS (dynamic light scattering) studies, revealing the particle size ranging from 80 to 200 nm, with an average hydrodynamic diameter of 131 nm (Fig. S20b, ESI†). Furthermore, an increase in the lifetime (ns) from 6.41 to 8.74 was noticed after the aggregate formation at f_w = 50% (Fig S20a and Table S5, ESI†). However, all these molecules displayed broad absorption at λ_{max} ∼ 440–450 nm (Fig. S21, ESI†) and intense emission at λ_{max} ∼ 530–550 nm in the solid state (Fig. 6a). The measured absolute quantum yields (Φ_f%) were remarkable for these solid probes (**TT1**: 55; **TT2**: 73, and **TT3**: 44) and would be valuable to employ them for handy and convenient strategies for pesticide detection.

The solid-state emission intensity depends on molecular packing, which depends on conformational flexibility and various supramolecular interactions. The multi-twisted molecular structures can suppress molecular proximity and thus induce radiative energy dissipation. The "V" shaped molecule **TT2**, containing sterically bulky groups, could exhibit enhanced solid-state emission, possibly due to its unique molecular arrangement in the solid state.[51] The **TT3**, and C_3-symmetric molecule possessing multiple flat anthracenes would possibly be involved in numerous supramolecular interactions, leading to relatively weaker emission. Nevertheless, these solid-state emitters were utilized to make a platform to detect the pesticides in a handy and convenient way. Such a dual-state detection-based probe offered superior results on sensing TN and FN compared to the existing literature (Table S6, ESI†).

Detection of pesticides using the solid-emitting platform

Solution-based detection is primarily suitable for laboratory settings, and it needs careful handling of sample preparation to avoid any spillage. To enable more convenient and user-friendly on-site applications, thin film-based detection is highly preferred. The **TT1**, **TT2**, and **TT3** (10^{-3} M in 1,4-dioxane) were separately drop-cast on Whatman filter paper (WP) (100% cellulose fibre) and dried at 298 K for 15 min to afford green-emitting platforms such as **TT1@WP**, **TT2@WP**, and **TT3@WP**. The dried paper strip **TT1@WP** was further characterised by IR and fluorescence studies (Fig. S22, ESI†) of the blank, before, and after exposure to TN solution (**TT1@WP** + TN). The IR spectrum of the blank was compared with **TT1**-casted paper (**TT1@WP**), demonstrating the appearance of new absorption signals at 1640 cm^{-1} (C=C), which were absent only in WP. For the emitting **TT1@WP**, solid platforms absorb at λ_{abs} = 450 nm, with corresponding emissions λ_{emi} = 538 nm. Furthermore, the emission of **TT1@WP** was quenched upon TN treatment, whereas no emission was observed for blank WP. These emitting platforms were treated with different pesticides, and respective changes are presented (Fig. S23, ESI†). Notably, **TT1** was green emissive in the solid state; these probes displayed strong quenching with TN and FN and a faint response against GP and IM. A very close contact of the dye and the pesticide within the porous filter paper could facilitate the interactions and result in efficient quenching responses. Upon exposure to pesticides, the 1640 cm^{-1} stretching remained intact in the IR spectra. However, no other vibration could be identified due to the lower concentration of TN (10^{-6} M). The emission at λ_{em} = 538 nm originated from **TT1@WP** and completely disappeared upon treatment with TN. The LOD was experimented with in the paper strip by dropping a solution of gradually diluted concentration (Fig. 7a and b). We could detect TN until 10^{-8} M and FN up to 10^{-7} M concentration using a **TT1**-coated paper strip. The **TT2** and **TT3** coated strips showed similar responses by recognizing TN until 10^{-5} M and FN up to 10^{-4} M concentration. The better responses with the **TT1** emitter are ascribed to suitable PET between closely spaced energy levels and the IFE event. Moreover, the crystalline nature of **TT1** compared to **TT2** and **TT3** (as noticed from PXRD profiles; Fig. S2, ESI†) was in favor of possessing suitable void space between the two molecular planes.
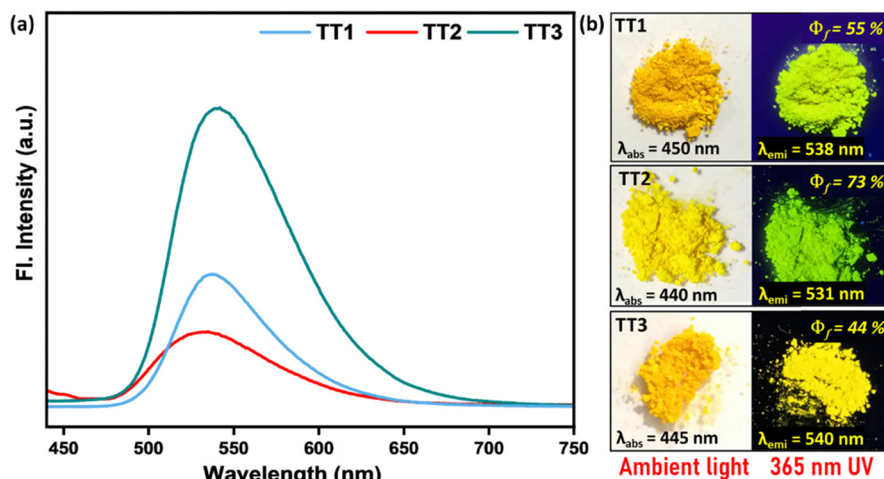
Fig. 6 (a) Emission spectra of **TT1**, **TT2** and **TT3** in the solid state, and (b) picture of **TT1**, **TT2**, and **TT3** in ambient light and 365 nm UV in the solid state.
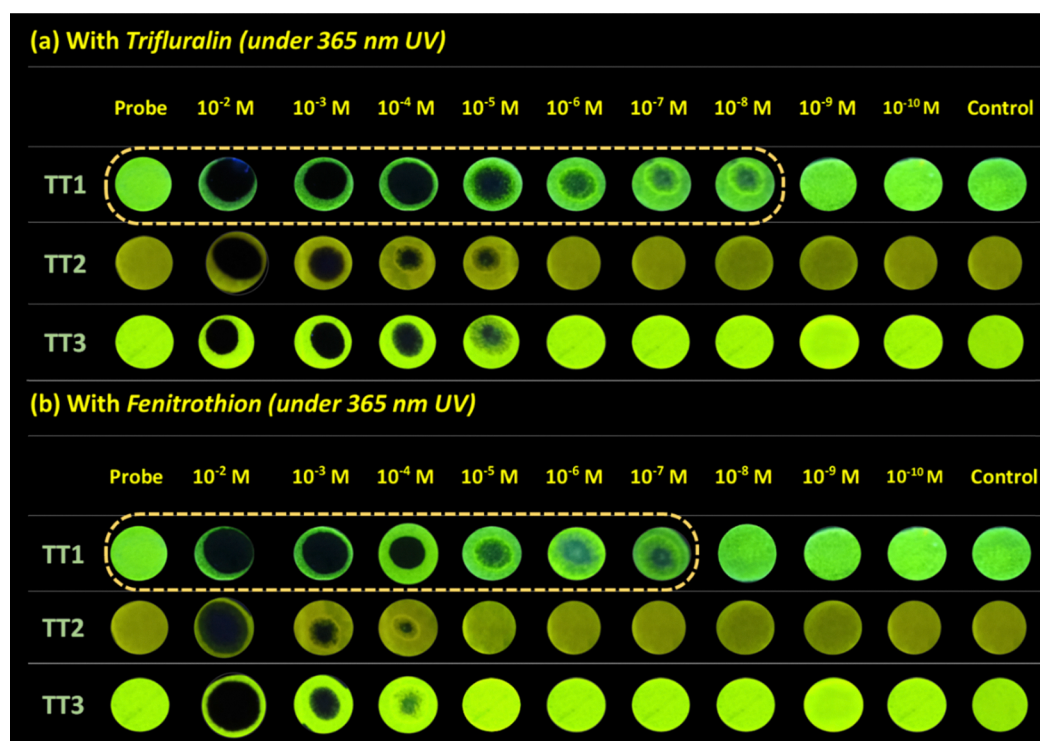

Fig. 7 **TT1@WP** (10 μM) was assessed before and after exposure to (a) TN and (b) FN with gradually diluted concentrations (under a 365 nm UV lamp).

Real-world applications

All these quenching events are visually detectable through the naked eye and thus further utilized for real-world on-site applications. Common non-expert people could monitor the solid-state emission quenching to detect pesticides from intense green emissions to dark, which would assist in recognizing pesticides using a 365 nm lamp without any expensive equipment. TN is the herbicide, widely used to control annual grasses and broadleaf weeds in various crops. It is typically applied to the soil to inhibit weed germination and growth.

It can easily leach into the groundwater from the soil and is highly toxic to aquatic life. Therefore, we first tested the presence of TN in farm/garden and grazing land soil samples. Each 3 g of soil was spiked with 0.5 mg, 1 mg, and 2 mg of TN to make $1.6 \times 10^{-4}\%$, $3.3 \times 10^{-4}\%$, and $6.6 \times 10^{-4}\%$ of TN/soil (w/w). The emission quenching of the probe was monitored by adding pesticide-spiked soil portion-wise ($\sim$10 mg of TN-spiked soil) into 2 mL of **TT1** solution. The quenching response was visually detected even with using $1.6 \times 10^{-4}\%$ (w/w) of TN in soil. However, no fluorescence quenching was observed
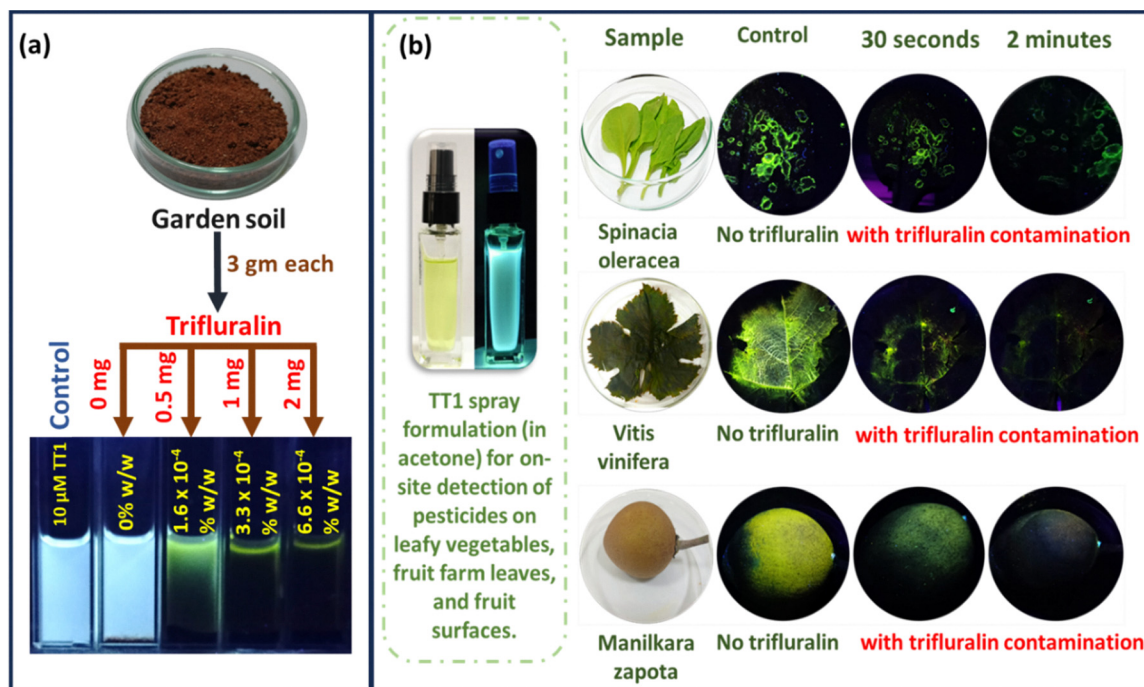
Fig. 8 TN detection in (a) garden soil and (b) **TT1** spray formulation (10 μM in acetone) for pesticide detection in leaves and fruit of various textures.

upon adding non-spiked soil samples (a control experiment was performed with the soil sample having no pesticides) (Fig. 8a). Hence, such detection of pesticides in soil would enable easy monitoring of toxic contaminants (such as TN) and protect cattle and terrestrial animals.

To evaluate the practical application of **TT1** as a fluorescent probe for detecting pesticide residues on various plant surfaces, a 10 μM solution of **TT1** in acetone was prepared and transferred into a spray bottle. This solution was applied to a selection of agricultural samples, including leafy vegetables (*Spinacia oleracea*), fruit leaves (*Vitis vinifera*), and fruits (*Manilkara zapota*), chosen for their diverse surface textures ranging from smooth to rough and uneven. To simulate pesticide contamination, these samples were treated with a 10 μM ethanol solution of TN by spraying it onto their surfaces. After allowing the TN solution to dry, the **TT1** solution was sprayed onto both the TN-treated and untreated (control) samples. Under illumination with a 365 nm UV lamp, the untreated areas exhibited a bright green fluorescence, indicating the

presence of **TT1**. In contrast, the TN-contaminated areas showed a noticeable quenching of fluorescence, with the green emission diminishing significantly within 30 to 120 seconds post-application. This rapid and visually discernible change in fluorescence intensity effectively distinguished between contaminated and uncontaminated surfaces (Fig. 8b). This experiment demonstrates the potential of **TT1**-formulated sprays as a practical, cost-effective, and user-friendly tool for the on-site detection of pesticide residues on various produce surfaces, contributing to food safety and environmental monitoring efforts. A schematic representation of the experiment is given as Fig. S24 (ESI†). Thus, we find an easy and convenient solution to detect TN and FN pesticides present in the soil, fruits, and vegetables of varying textures.

Furthermore, **TT1**-coated fluorescent cotton buds were fabricated (Fig. S25, ESI†) as a handy on-site pesticide detector (Fig. 9). The cotton buds will be rubbed on the surface, and based on the emission reduction, the presence of TN or FN pesticides can be quickly and comfortably tested on-site. This
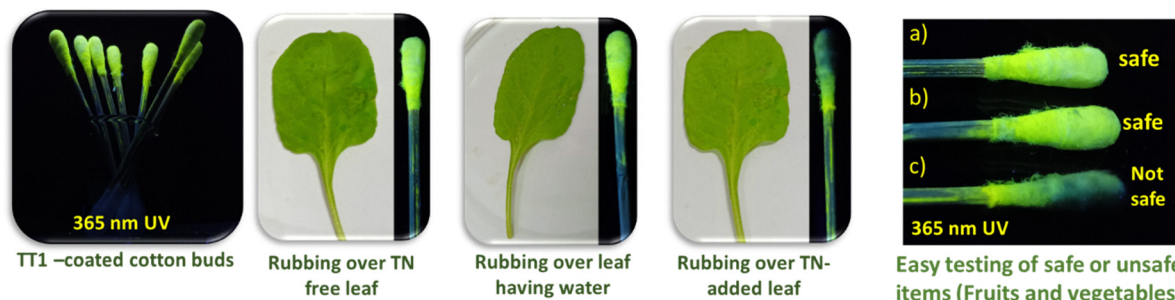

Fig. 9 **TT1**-coated fluorescent cotton buds as a handy on-site pesticide detector.

method for pesticide detection is particularly effective for analysing household kitchen samples, especially on smooth surfaces. It facilitates the identification of pesticide residues commonly found in domestic environments, particularly useful for households aiming to monitor and ensure the safety of their kitchen environments by detecting potential pesticide contamination on smooth surfaces of leafy vegetables, fruits, and vegetable surfaces.

Conclusion

In summary, this study presents a series of multi-twisted TPA–anthracene linked π-conjugates, namely **TT1**, **TT2**, and **TT3**, that exhibit excellent dual-state fluorescence profiles. Interestingly, the smallest analogue **TT1** with the least number of TPA/anthracene units demonstrates AIEE characteristics. These molecules have been employed as efficient and highly selective dual-state fluorescent detectors for pesticides. Upon interaction with specific pesticides TN and FN, fluorescence dimming is observed, with an appreciable detection limit in the range of 180 nM for TN and 320 nM for fenitrothion (FN) in solution, and in the 10^{-8} M range for solid-phase detection. The quenching mechanisms are attributed to PET and IFE, involving both dynamic and static quenching. For practical applications, **TT1** has been formulated into sprays and fabricated onto cotton buds, facilitating real-life sample analysis. These tools have been effectively utilized for on-site detection of pesticide residues in various environments, including garden soil (representing grazing lands) and post-farm samples with diverse surface textures (smooth, rough, and uneven). This highlights the potential of well-defined small organic molecules in developing cost-effective, user-friendly, and sustainable analytical tools for environmental monitoring and food safety. The integration of AIEE-active TPA units into small molecular frameworks offers a promising avenue for future research in the development of fluorescent probes and sensors.

Methods

All the fluorophores were synthesized using a method reported earlier. The electronic absorption spectra were recorded with a UV 3600 Plus (Shimadzu). The emission spectra were recorded using a Hitachi spectrofluorometer (F7000) using a 1 cm path-length quartz cuvette. Origin Pro 8.5 software is used to plot the obtained data.

Measurements and instrumentations

Thermal analysis study

Thermogravimetric analysis (TGA) was conducted on Shimadzu DTG-60 simultaneous DTA-TG apparatus with an increasing temperature rate at 5 °C min^{-1} in a N$_2$ atmosphere.

Steady-state absorption and fluorescence measurements

The electronic absorption spectra in the solution state were recorded with a UV 3600 Plus (Shimadzu) spectrophotometer.

The wavelength range was kept within 550 to 200 nm. The fluorescence spectra were recorded on a Hitachi spectrofluorometer (F7000, Japan) using a 1 cm path-length quartz cuvette. A stock solution of **TT1**, **TT2**, and **TT3** of 10^{-3} M was prepared in 1,4-dioxane and was further diluted, and pesticide stock solutions were made of 10^{-3} M (trifluralin, fenitrothion, diphenylamine, chlorpyrifos, β-cyfluthrin and imidacloprid in 1,4-dioxane), (glyphosate in water). The final concentration of the **TT1**, **TT2** and **TT3** was adjusted to 10 μM. The solid-state absorption and emission spectra were recorded for the as-synthesized samples.

Preparation of pesticide solutions and titration

The pesticides were solubilised in trifluralin, fenitrothion, diphenylamine, chlorpyrifos, β-cyfluthrin and imidacloprid in 1,4-dioxane (glyphosate in water). Furthermore, the absorption and emission spectra were recorded for **TT1**, **TT2** and **TT3** (10 μM in 1,4-dioxane), followed by adding different fractions (volumes) of pesticides from a stock solution.

Solid-state absorption measurement

The solid-state absorbance of the powder samples was measured using a Jasco V-650 UV-vis spectrophotometer equipped with a PSH-002 powder sample holder. Powder samples were finely ground and prepared to a uniform thickness ranging from 0.5 mm to 6 mm with a diameter of 16 mm. The instrument was first calibrated using a white diffuse reflectance standard (BaSO$_4$) to set the baseline transmittance. The powder samples were then placed into the powder sample holder, ensuring an even and flat surface.

Paper strip quenching study

TT1@WP was treated with different pesticide solutions (10^{-3} M) and was dropped *via* micropipette over **TT1@WP**. Additionally, for titration, a similar method was employed with different concentrations of amine (10^{-2} M to 10^{-10} M), and the pictures were captured in ambient light under a 365 nm UV lamp using a cell phone camera.

Lifetime decay measurement. Time-resolved fluorescence measurements were performed using a time-correlated single-photon counting (TCSPC) unit (Horiba Deltaflex). The laser used for all samples was 440 nm with a setup target of 10 000 counts. Ludox solution (an aqueous dispersion of colloidal silica) was used to measure the IRF for all solution samples. All measurements were performed at room temperature (298 K). The decay fitting was completed, keeping the χ^2 value close to unity.

Powder X-ray diffraction measurement. PXRD measurements were carried out using a Xenocs Nano-in Xider SW-L SAXS/WAXS system with a dual detector with Cu Kα micro focus within the range of 5° to 50° at a scanning speed of 2° min^{-1}. The sample was placed and spread over a Kapton tape, and data were recorded in transmission geometry.

Absolute quantum yield measurement

The solid-state absolute quantum yield was measured using a calibrated integrating fully assembled 3.2-inch diameter

K-sphere method with a fluorimeter (Fluorolog, HORIBA), with an absolute error of ±0.25%.

NMR titration study

The experiment was conducted in CDCl₃ (0.5 mL) by adding TN (1 equivalent) to 6 mg **TT1**.

Infrared spectroscopic studies

The IR spectra were recorded using an FT-IR spectrometer using ATR-FT-IR spectra.

Theoretical study and computational details

All the calculations were performed in Gaussian using B3LYP-D3(BJ)/6-31G** (with dispersion corrections).

Author contributions

The manuscript was written through the contributions of all authors. All authors have given approval to the final version of the manuscript.

Conflicts of interest

There are no conflicts to declare.

Data availability

The data supporting this article have been included as part of the ESI.†

Acknowledgements

References

1 Z. Liu, J. Zeng, D. Wang, P. Zhu, L. Wang, Y. Bao, Y. Xu, W. Peng, S. He, Z. Lei and L. Pang, Spiro-Linked Planar Core Small Molecule Hole Transport Materials Enabling High-Performance Inverted Perovskite Solar Cells, *J. Am. Chem. Soc.*, 2025, **147**, 12345–12356.

2 S. Li, J. Lin, X. Chen, W. Liu, Z. Xie, C. Zeng, J. Wang, Y. Min and X. Feng, Pyrene-Based Triphenylamine Light-Harvesting Materials with Related Structure–Property Relationships, *J. Org. Chem.*, 2025, **90**, 2345–2356.

3 A. Staoui, A. Idrissi, Z. El Fakir and S. Bouzakraoui, Efficient Thiophene-Based Hole Transport Materials Containing Amide Groups as Bridges and Thiophene Derivatives as Acceptors for Perovskite Solar Cells, *ACS Appl. Energy Mater.*, 2025, **8**, 3456–3467.

4 M. Panneerselvam, A. Kathiravan, R. V. Solomon and M. Jaccob, The Role of π-Linkers in Tuning the Optoelectronic Properties of Triphenylamine Derivatives for Solar Cell Applications – A DFT/TDDFT Study, *Phys. Chem. Chem. Phys.*, 2017, **19**, 6153–6163.

5 S. Goker, S. O. Hacioglu, G. Hizalan, E. Aktas, A. Cirpan and L. Toppare, Triphenylamine Based Random Copolymers: The Effect of Molecular Weight on Performance of Solar Cell and Optoelectronic Properties, *Macromol. Chem. Phys.*, 2017, **218**, 1600544.

6 L. Wu, J. Xu, Z. Zhang, W. Xue, T. Wang, C. Yan, J. He, Y. He, H. Yan and H. Meng, Fused Triphenylamine Moiety Based Fluorescence Emitters for Deep Blue OLEDs, *Adv. Funct. Mater.*, 2025, **35**, 4567–4578.

7 P. Cias, C. Slugovc and G. Gescheidt, Hole Transport in Triphenylamine Based OLED Devices: From Theoretical Modeling to Properties Prediction, *J. Phys. Chem. A*, 2011, **115**, 14519–14525.

8 P. S. Hariharan, N. S. Venkataramanan, D. Moon and S. P. Anthony, Self-Reversible Mechanochromism and Thermochromism of a Triphenylamine-Based Molecule: Tunable Fluorescence and Nanofabrication Studies, *J. Phys. Chem. C*, 2015, **119**, 9460–9469.

9 C. Hamciuc, E. Hamciuc, M. Homocianu, A. Nicolescu and G. Lisa, New Blue Fluorescent and Highly Thermostable Polyimide and Poly(amide-imide)s Containing Triphenylamine Units and (4-Dimethylaminophenyl)-1,3,4-Oxadiazole Side Groups, *Dyes Pigm.*, 2018, **148**, 249–262.

10 J. Pina, J. S. Seixas de Melo, R. M. Batista, S. P. Costa and M. M. M. Raposo, Triphenylamine–Benzimidazole Derivatives: Synthesis, Excited-State Characterization, and DFT Studies, *J. Org. Chem.*, 2013, **78**, 11389–11395.

11 J. H. Kim, J. H. Yun and J. Y. Lee, Recent Progress of Highly Efficient Red and Near-Infrared Thermally Activated Delayed Fluorescent Emitters, *Adv. Opt. Mater.*, 2018, **6**, 1800255.

12 P. S. Hariharan, V. K. Prasad, S. Nandi, A. Anoop, D. Moon and S. P. Anthony, Molecular Engineering of Triphenylamine Based Aggregation Enhanced Emissive Fluorophore: Structure-Dependent Mechanochromism and Self-Reversible Fluorescence Switching, *Cryst. Growth Des.*, 2017, **17**, 146–155.

13 N. Nirmalananthan-Budau, J. H. Budau, D. Moldenhauer, G. Hermann, W. Kraus, K. Hoffmann, B. Paulus and U. Resch-Genger, Substitution Pattern Controlled Aggregation-Induced Emission in Donor–Acceptor–Donor Dyes with One and Two Propeller-like Triphenylamine Donors, *Phys. Chem. Chem. Phys.*, 2020, **22**, 14142–14154.

14 H. T. Lin, C. L. Huang and G. S. Liou, Design, Synthesis, and Electrofluorochromism of New Triphenylamine Derivatives with AIE-Active Pendent Groups, *ACS Appl. Mater. Interfaces*, 2019, **11**, 11684–11690.

15 Y. Yan, N. Sun, F. Li, X. Jia, C. Wang and D. Chao, Multiple Stimuli-Responsive Fluorescence Behavior of Novel Polyamic Acid Bearing Oligoaniline, Triphenylamine, and Fluorene Groups, *ACS Appl. Mater. Interfaces*, 2017, **9**, 6497–6503.

16 D. Bokotial, S. Bhattacharyya, S. Arunkumar, T. Das, G. R. M. Rajendran and A. Chowdhury, Multi Stimuli

Responsive Dual Aggregation-Induced Emission and Photochromic Behavior of a Tetraphenyl Substituted Triphenylamine Derivative and Its Application as Anti-Counterfeiting Agent, *Chem. – Eur. J.*, 2024, **30**, 202402086.

17 Y. Huang, L. Ning, X. Zhang, Q. Zhou, Q. Gong and Q. Zhang, Stimuli-Fluorochromic Smart Organic Materials, *Chem. Soc. Rev.*, 2024, **53**, 1090–1166.

18 Z. Lv, Z. Man, Z. Xu, L. Fu, S. Li, Y. Zhang and H. Fu, High Contrast and Bright Emission Piezochromic Fluorescence in Organic Crystals via Pressure Modulated Exciton Coupling Effect, *Adv. Opt. Mater.*, 2021, **9**, 2100598.

19 W. Zhou, M. Li and V. Achal, A Comprehensive Review on Environmental and Human Health Impacts of Chemical Pesticide Usage, *Emerging Contam.*, 2024, **10**, 100410.

20 P. Elumalai, X. Gao, P. Parthipan, J. Luo and J. Cui, Agrochemical Pollution: A Serious Threat to Environmental Health, *Curr. Opin. Environ. Sci. Health*, 2025, 100597.

21 F. H. Tang, M. Lenzen, A. McBratney and F. Maggi, Risk of Pesticide Pollution at the Global Scale, *Nat. Geosci.*, 2021, **14**, 206–210.

22 L. Xu, A. M. Abd El-Aty, J. B. Eun, J. H. Shim, J. Zhao, X. Lei, S. Gao, Y. She, F. Jin, J. Wang and M. Jin, Recent Advances in Rapid Detection Techniques for Pesticide Residue: A Review, *J. Agric. Food Chem.*, 2022, **70**, 13093–13117.

23 C. Chouteau, S. Dzyadevych, C. Durrieu and J. M. Chovelon, A Bi-Enzymatic Whole Cell Conductometric Biosensor for Heavy Metal Ions and Pesticides Detection in Water Samples, *Biosens. Bioelectron.*, 2005, **21**, 273–281.

24 F. Sahin, N. Celik, A. Camdal, M. Sakir, A. Ceylan, M. Ruzi and M. S. Onses, Machine Learning-Assisted Pesticide Detection on a Flexible Surface-Enhanced Raman Scattering Substrate Prepared by Silver Nanoparticles, *ACS Appl. Nano Mater.*, 2022, **5**, 13112–13122.

25 P. Viñas, N. Campillo, I. López-García, N. Aguinaga and M. Hernández-Córdoba, Capillary Gas Chromatography with Atomic Emission Detection for Pesticide Analysis in Soil Samples, *J. Agric. Food Chem.*, 2003, **51**, 3704–3708.

26 A. Samsidar, S. Siddiquee and S. M. Shaarani, A Review of Extraction, Analytical and Advanced Methods for Determination of Pesticides in Environment and Foodstuffs, *Trends Food Sci. Technol.*, 2018, **71**, 188–201.

27 S. B. Ravikumar, T. A. Mallu, S. Subbareddy, S. A. Shivamurthy, V. D. Neelalochana, K. C. Shantakumar, J. R. Rajabathar, N. Ataollahi and S. Shadakshari, An Enhanced Non-Enzymatic Electrochemical Sensor Based on the Bi_2S_3–TiO_2 Nanocomposite with HNTs for the Individual and Simultaneous Detection of 4-Nitrophenol and Nitrofurantoin in Environmental Samples, *J. Mater. Chem. B*, 2024, **12**(36), 9005–9017.

28 M. Palanna, M. Itagi, L. K. Sannegowda, B. Kulkarni, K. Hiremath, M. Austeria and R. G. Balakrishna, A Bio-Mimicking Cobalt Tetramenthol-Substituted Phthalocyanine-Based Electrochemical Sensor for Selective and Sensitive Detection of tert-Butylhydroquinone, *J. Mater. Chem. B*, 2025, **13**(13), 4188–4200.

29 Y. Chen, W. Gu, C. Zhu and L. Hu, Recent Advances in Photoelectrochemical Sensing for Food Safety, *Anal. Chem.*, 2024, **96**, 8855–8867.

30 L. Gao, L. Ju and H. Cui, Chemiluminescent and Fluorescent Dual-Signal Graphene Quantum Dots and Their Application in Pesticide Sensing Arrays, *J. Mater. Chem. C*, 2017, **5**(31), 7753–7758.

31 M. Bhattu, M. Verma and D. Kathuria, Recent Advancements in the Detection of Organophosphate Pesticides: A Review, *Anal. Methods*, 2021, **13**, 4390–4428.

32 S. Shanmugaraju, K. Giriraj, A. Shanmughan, Y. Jegadeesan, M. K. Noushija, V. K. Alenthwar, H. Gangadharan and U. Deivasigamani, Recent Progress in Fluorescence-Based Chemosensing of Pesticides, *Sens. Diagn.*, 2025, **4**, 1234–1256.

33 D. An, L. Chen, Y. Liang, J. Hou and J. Chen, Defect-Containing Metal–Organic Framework Materials for Sensor Applications, *J. Mater. Chem. A*, 2024, **12**(1), 38–58.

34 L. Qin, Y. Guo, L. Li, D. Lin, Y. Li, S. Xu and C. Jiang, Ratiometric Fluorescent Sensor Based on Hydrogen-Bond Triggering the Internal Filter Effect for Enzyme-Free and Visual Monitoring Pesticide Residues, *ACS Sustainable Chem. Eng.*, 2023, **11**, 11032–11040.

35 Z. Zheng, K. Li, S. Wang, H. Zhao, X. Yang, Y. Niu, M. Li, X. Luo, Z. Li and W. Tang, Development of a Zr/Fe-MIL Nanozyme Sensor Integrated with a User-Friendly Colorimetric Device for Glyphosate Monitoring, *Anal. Methods*, 2025, **17**, 4538–4547.

36 S. Shanmugaraju, K. Giriraj, A. Shanmughan, Y. Jegadeesan, M. K. Noushija, V. K. Alenthwar, H. Gangadharan and U. Deivasigamani, Recent Progress in Fluorescence-Based Chemosensing of Pesticides, *Sens. Diagn.*, 2025, **4**, 460–488.

37 S. Razzaque, M. Abubakar, M. A. Farid, R. Zia, S. Nazir, H. Razzaque, A. Ali, Z. Ali, A. Mahmood, W. Al-Masry and T. Akhter, Detection of Toxic Cypermethrin Pesticides in Drinking Water by Simple Graphitic Electrode Modified with Kraft Lignin@Ni@gC_3N_4 Nano-Composite, *J. Mater. Chem. B*, 2024, **12**(37), 9364–9374.

38 A. Sarma, S. Ghosh and S. Biswas, An Aluminium–Organic Framework Unveiling Ultra-Sensitive Fluorometric Detection of Pesticide Paraoxon-Methyl and Pharmaceutical Drug Azathioprine in Fruits, Vegetables, and Wastewater, *J. Mater. Chem. C*, 2024, **12**(35), 13892–13903.

39 I. Mukherjee, T. Basu and L. M. Bharadwaj, Metal Organic Framework Steered Electrosynthesis of Anisotropic Gold Nanorods for Specific Sensing of Organophosphate Pesticides in Vegetables Collected from the Field, *Nanoscale*, 2020, **12**, 21719–21733.

40 Y. Gu, X. Pu, J. Chen, L. Yi, J. Bi, F. Duan and K. Ge, Recent Advances of MOF-Based SERS Substrates in Quantitative Analysis of Food Contaminants: A Review, *Analyst*, 2024, **149**, 4997–5013.

41 J. Song, S. Wu, P. Xing, Y. Zhao and J. Yuan, Di-Branched Triphenylamine Dye Sensitized TiO_2 Nanocomposites with Good Photo-Stability for Sensitive Photoelectrochemical Detection of Organophosphate Pesticides, *Anal. Chim. Acta*, 2018, **1001**, 24–31.

42 B. Zhang, J. Yan, Y. Shang and Z. Wang, Synthesis of Fluorescent Micro- and Mesoporous Polyaminals for Detection of Toxic Pesticides, *Macromolecules*, 2018, **51**, 1769–1776.

43 S. Sau, F. Banerjee and S. K. Samanta, Triphenylamine–Anthracene-Based Conjugated Microporous Polymers for the Detection and Photocatalytic Degradation of Organic Micropollutants, *ACS Appl. Nano Mater.*, 2023, **6**, 11679–11688.

44 S. Tripathi and M. Chakravarty, Unveiling the Long-Awaited Aldehyde Intermediate in Oxidative Dephosphorylation: A Unique Approach to Access Useful Carboxaldehydes, *Chem. – Eur. J.*, 2025, **31**, 202403300.

45 G. I. McGrew, J. Temaismithi, P. J. Carroll and P. J. Walsh, A Novel Approach to Polyarylated Methanes via Cross-Coupling of Tricarbonylchromium-Activated Benzyl-lithiums, *Angew. Chem., Int. Ed.*, 2010, **49**, 5541–5544.

46 S. Tripathi, S. Halder, P. Sivasakthi, P. K. Samanta, C. Chakraborty and M. Chakravarty, Sidearms Elongated C3-Symmetric Electrochromic and Electrofluorochromic π-Conjugate: Small Molecule in Efficient Transparent to Black Switching, *Next Mater.*, 2025, **6**, 100472.

47 J. Mei, N. L. C. Leung, R. T. Kwok, J. W. Y. Lam and B. Z. Tang, Aggregation-Induced Emission: Together We Shine, United We Soar!, *Chem. Rev.*, 2015, **115**, 11718–11940.

48 J. Voskuhl and M. Giese, Mesogens with Aggregation-Induced Emission Properties: Materials with a Bright Future, *Aggregate*, 2022, **3**, 124.

49 B. Prusti and M. Chakravarty, Disparity in Piezofluorochromism for Twisted Mono-Carbazole-Based AIEgens Resulting from Interchanging Electron-Rich Substituents: Effect of Coplanarity on Twisted π-Conjugates, *Mater. Adv.*, 2021, **2**, 1752–1759.

50 B. Prusti, P. Sarkar, S. K. Pati and M. Chakravarty, Multistimuli and Fingertip Triggered Luminescence Switching: A Five Colored Ink Free Rewritable Secured Platform with Strongest Red Emission, *J. Mater. Chem. C*, 2021, **9**, 9555–9570.

51 G. Gopan, P. S. Salini, S. Deb and M. Hariharan, V-Shaped Oxydiphthalimides: Side-Chain Engineering Regulates Crystallisation-Induced Emission Enhancement, *CrystEngComm*, 2017, **19**, 419–425.